POLITECNICO DI TORINO
Repository ISTITUZIONALE

Fine color-tuning of Ir(iii) tetrazolato complexes: synthesis, photophysical properties and OLED device fabrication

Original
Fine color-tuning of Ir(iii) tetrazolato complexes: synthesis, photophysical properties and OLED device fabrication / Monti, N., Previati, E., Vigarani, G., Cocchi, M., Tinti, F., Raiteri, P., Zacchini, S., Giorgini, L., Massi, M., Stagni, S., Fiorini, V.. - In: DALTON TRANSACTIONS. - ISSN 1477-9234. - ELETTRONICO. - 54:26(2025), pp. 10304-10317. [10.1039/D4DT03525A]

Availability:
This version is available at: 11583/3001794 since: 2025-07-12T06:08:46Z

Publisher:
Royal Society of Chemistry

Published
DOI:10.1039/D4DT03525A

Terms of use:

This article is made available under terms and conditions as specified in the corresponding bibliographic description in the repository

Publisher copyright

(Article begins on next page)

13 September 2026

Dalton Transactions

ROYAL SOCIETY OF CHEMISTRY

PAPER

View Article Online
View Journal | View Issue

Check for updates

Cite this: *Dalton Trans.*, 2025, **54**, 10304

Fine color-tuning of Ir(III) tetrazolato complexes: synthesis, photophysical properties and OLED device fabrication†

Nicola Monti, [a] Eleonora Previati, [a,e] Giulia Vigarani, [a] Massimo Cocchi, [b] Francesca Tinti, [b] Paolo Raiteri, [c] Stefano Zacchini, [a] Loris Giorgini, [a] Massimiliano Massi, [d] Stefano Stagni *[a] and Valentina Fiorini *[a]

Received 23rd December 2024,
Accepted 12th May 2025

DOI: 10.1039/d4dt03525a

rsc.li/dalton

The preparation of a new series of Ir(III) tetrazolato complexes with the general formula **[Ir(C^N)$_2$(N^N)]$^{0/+}$**, where the ancillary ligand (N^N) is represented in turn by 2-pyridyltetrazolato (**PTZ$^-$**), 2-pyrazinyltetrazolato (**PYZ$^-$**) or 2-pyridyl 5-trifluoromethyl tetrazolato (**PTZ-CF$_3^-$**), is described herein. The design of the cyclometalated (C^N) ligands, namely 2-phenylisonicotinonitrile (**ppyCN**) and 2-(2,4-difluorophenyl)isonicotinonitrile (**F$_2$ppy-CN**), features the well-known **ppy**- or **F$_2$ppy** core, with the introduction of one electron-withdrawing cyano (–CN) group at the *para* position of the pyridyl ring. The photophysical and electrochemical properties of the new Ir(III) cyclometalated complexes have been investigated and the resulting data suggest how the (C^N) ligands significantly rule the luminescence behavior of the new complexes. Further blue or red shifting of the emission profiles of the neutral complexes was observed upon their conversion into cationic species through the regioselective addition of a methyl moiety to the coordinated tetrazolato ring. Lastly, neutral **[Ir(F$_2$ppy-CN)$_2$(PTZ)]** was used as an emissive phosphor for the fabrication of an **OLED**-type device.

Open Access Article. Published on 13 May 2025. Downloaded on 7/11/2025 6:28:05 AM.
This article is licensed under a Creative Commons Attribution-NonCommercial 3.0 Unported Licence.

Introduction

The scientific success of photoactive and chemically stable Ir(III)-cyclometalated complexes is witnessed by the ongoing development of their applicative scenario, which has been extended to optical imaging[1] and more recently to the field of photocatalysis.[2a–d] However, solid state lighting can still be regarded as the core application for this class of compounds, which have been used as brightly emissive materials for the fabrication of both OLED (Organic Light Emitting Diode)[3] and LEEC (Light Emitting Electrochemical Cell) electroluminescent devices.[4] Among the several key factors on which is based the privileged role of Ir(III) cyclometalates for all the aforementioned applications,[5] the chance of chemically modulating the luminescence output is of extreme importance. Both homoleptic *fac*-[Ir(C^N)$_3$] and heteroleptic **[Ir(C^N)$_2$(N^N)]$^{+/0/-}$** varieties can be customized to produce emissions spanning from blue to the NIR region through rational modifications of the ligand set.[6a–c] This also includes the research based on tetrazole and tetrazolato Ru(II),[7a,b] Re(I)[8a–c] and Ir(III) complexes, one of our primary interest. The flexibility of this class of nitrogen-rich ligands is what underlies the structure–property relationships of tetrazole-based Ir(III) complexes, which are closely related to both the nature of the tetrazole ligand used[9] and the net charge of the resulting complex.[8a,10a–c] Relative to all the Ir(III) complexes that we have reported so far, in which the set of (C^N) ligands was steadily constituted by a phenylpyridinato anion (ppy$^-$) or its fluorinated analogue (**F$_2$ppy$^-$**), the chemical modifications (both permanent and reversible) performed on the tetrazolato ligand (N^N) did result in the red shift of the emission profiles, with an extent that is strictly correlated to the nature of the 5-aryl substituent of the tetrazolato ring.[9,10a,c] In this work, we investigate how the concomitant modification of the (C^N) ligands can influence and further modulate the luminescence output of cyclometalated Ir(III) tetrazolato complexes. For doing this, the (C^N) ligands were modified by introducing the electron-withdrawing nitrile

[a]*Department of Industrial Chemistry "Toso Montanari", University of Bologna, Via Gobetti 85, 40129 Bologna, Italy. E-mail: stefano.stagni@unibo.it*
[b]*Institute for Organic Synthesis and Photoreactivity, CNR, via Gobetti 101, 40129 Bologna, Italy*
[c]*Curtin Institute for Computation and School of Molecular and Life Sciences, Curtin University, P.O. Box U1987, Perth, WA 6845, Australia*
[d]*Curtin Institute for Functional Molecules and Interfaces, School of Molecular and Life Science, Curtin University, Kent Street, Bentley 6102, WA, Australia*
[e]*Department of Applied Science and Technology-DISAT, Politecnico di Torino, Corso Duca degli Abruzzi 24, 10129 Torino, Italy*

†Electronic supplementary information (ESI) available. CCDC 2411033. For ESI and crystallographic data in CIF or other electronic format see DOI: https://doi.org/10.1039/d4dt03525a

This journal is © The Royal Society of Chemistry 2025

Open Access Article. Published on 13 May 2025. Downloaded on 7/11/2025 6:28:05 AM.
This article is licensed under a Creative Commons Attribution-NonCommercial 3.0 Unported Licence.

group (–CN) at the *para* position of the pyridyl ring, where usually the LUMO level is mainly localized.[5,6a] To this extent, herein we report the synthesis and the spectroscopic and electrochemical characterization of a new family of **[Ir(C^N)$_2$(N^N)]** complexes, in which (C^N) represents 2-phenylisonicotinonitrile (**ppyCN**) or 2-(2,4-difluorophenyl)isonicotinonitrile (**F$_2$ppy-CN**), while (N^N) represents 2-pyridyl tetrazolato (**PTZ$^-$**), its –CF$_3$ substituted analogue (**PTZ-CF$_3$$^-$**) or the 2-pyrazinyl based derivative (**PYZ$^-$**). By exploiting the reactivity through electrophiles displayed by the coordinated pentatomic ring, we have prepared the corresponding **[Ir(C^N)$_2$(N^N)]$^+$** complexes that exhibited unexpected photophysical properties with respect to those previously observed. Furthermore, neutral **[Ir(F$_2$ppy-CN)$_2$(PTZ)]** was explored as an emissive phosphorescent material in the fabrication of an organic light-emitting diode.

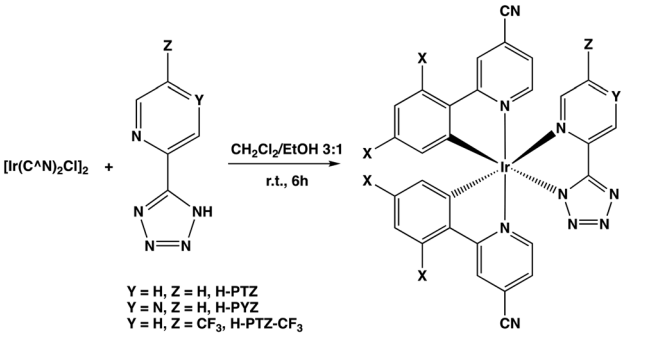

Scheme 2 Synthesis of the neutral Ir(III) complexes reported in this work.

Results and discussion

The cyano-substituted cyclometalating ligands were synthesized through standard Suzuki–Miyaura coupling involving the appropriate phenyl or 2,4 difluorophenyl boronic acid and 4-cyano 2-bromo pyridine.[11] The formation of the dichloro-bridged Ir(III) dimer precursor **[Ir(ppy-CN)$_2$Cl]$_2$** was then achieved according to the procedure reported by Nonoyama and coworkers.[12] Instead, a longer reaction time (48 h) and pure ethoxyethanol as the solvent were required for **[Ir(F$_2$ppy-CN)$_2$Cl]$_2$** (Scheme 1).

The heteroleptic neutral Ir(III) complexes were obtained under mild conditions by reaction of the Ir(III) dimers with a slight excess of the appropriate tetrazole ligand (Scheme 2).[9,10] Pure samples of the targeted compounds were obtained through column chromatography. The identity of each complex was confirmed by ESI-MS and NMR spectroscopy (^{1}H, ^{13}C), which provided the results in complete agreement with previously reported Ru(II) and Ir(III) tetrazolato and tetrazole complexes (see the ESI† for further details).[7a,b,8a,9,10a–c] For all the neutral complexes reported, the coordination of the tetrazolato ligand to the metal centre through its N-1 position was confirmed by the ^{13}C-resonance of the tetrazolato carbon (C$_t$) between 162 and 165 ppm (Scheme 3, ESI S1–S24†).

Each neutral Ir(III) complex was then converted into the corresponding cationic analogue by reaction with a slight excess of methyl triflate (Scheme 3). All the methylated complexes displayed one single C$_t$ resonance which, with respect to that observed for their neutral precursors, appeared shifted downfield (δC$_t$ = *ca.* 166–168 ppm). As we demonstrated earlier, this effect is congruent with the regioselective addition of a methyl group to the less sterically demanding N-3 position of the Ir(III)-coordinated tetrazolate ring (Scheme 3).[9,10a–c]

X-ray crystallography

The evidence deduced from ^{1}H/^{13}C NMR experiments were further confirmed from the X-ray diffraction of **[Ir(ppyCN)$_2$(PTZ-CF$_3$)]**. The molecular structure of **[Ir(ppyCN)$_2$(PTZ-CF$_3$)]** (Fig. 1) is similar to that of previously reported [Ir(C^N)$_2$(N^N)] complexes.[9,10a–c] Thus, it contains a distorted octahedral Ir(III) centre with *cis*-metalated carbons and *trans*-phenylpyridine nitrogen atoms. The Ir–N (N^N) distances (2.108(14) and 2.169(16) Å) are longer than Ir–N (C^N) (2.022(17) and 2.028(18) Å) because of the *trans* influence of the metalated carbon atoms. The PTZ-CF$_3$ ligand is almost coplanar (mean deviation from the least square plane 0.0601 Å).

Photophysical properties

The absorption spectra of all the neutral and cationic Ir(III) species were obtained from diluted (10^{-5} M) CH$_3$CN solutions

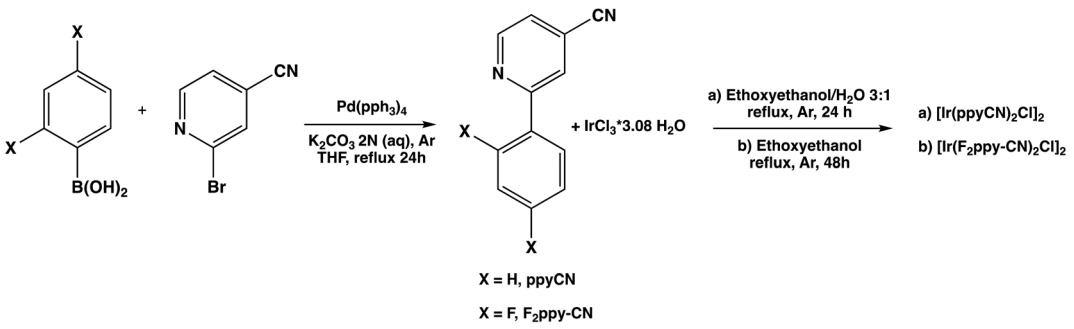

Scheme 1 Synthesis of **[Ir(ppyCN)$_2$Cl]$_2$** and **[Ir(F$_2$ppy-CN)$_2$Cl]$_2$**.

Open Access Article. Published on 13 May 2025. Downloaded on 7/11/2025 6:28:05 AM.
This article is licensed under a Creative Commons Attribution-NonCommercial 3.0 Unported Licence.

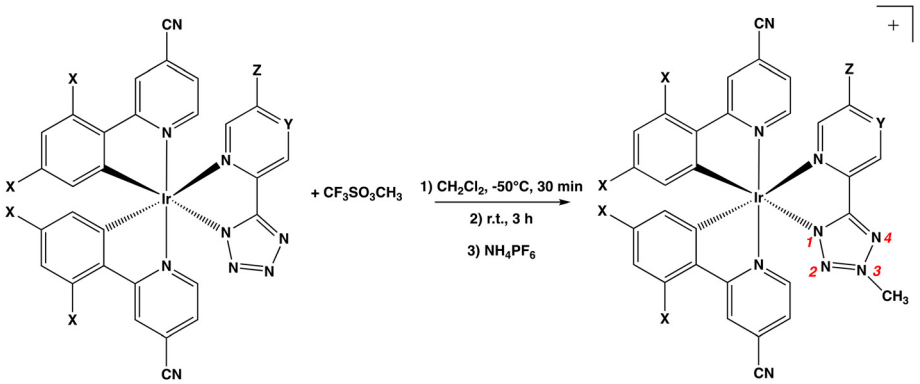

Scheme 3 Methylation reaction of Ir(III) compounds with relative acronyms and numeration of the tetrazolato ring used in this work.

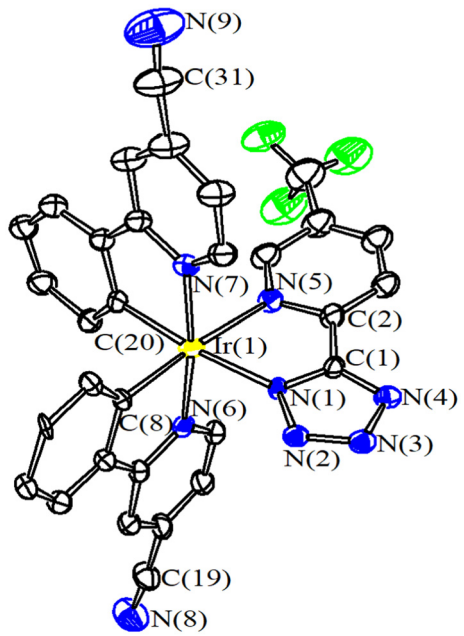

Fig. 1 Molecular structure of **[Ir(ppyCN)$_2$(PTZ-CF_3)]** with the key atoms labelled. H-atoms have been omitted for clarity. Displacement ellipsoids are at the 30% probability level. Selected bond lengths (Å) and angles (°): Ir(1)–N(1) 2.108(14), Ir(1)–N(5) 2.169(16), Ir(1)–N(6) 2.022(17), Ir(1)–N(7) 2.028(18), Ir(1)–C(8) 2.032(18), Ir(1)–C(20) 2.04(2), C(1)–N(1) 1.33(2), N(1)–N(2) 1.34(2), N(2)–N(3) 1.30(2), N(3)–N(4) 1.35(2), N(4)–C(1) 1.32(3), C(1)–C(2) 1.45(3), C(19)–N(8) 1.15(3), C(31)–N(9) 1.16(4), N(1)–Ir(1)–C(20) 173.9(7), N(7)–Ir(1)–N(6) 172.0(7), N(5)–Ir(1)–C(8) 174.2(7). N(1)–Ir(1)–N(5) 76.2(6), C(1)–N(1)–N(2) 139.6(12), N(1)–N(2)–N(3) 108.6(16), N(2)–N(3)–N(4) 110.8(17), N(3)–N(4)–C(1) 102.9(17), N(1)–C(1)–N(4) 127.2(19).

at 298 K. In all cases, the absorption profile consists of intense ^{1}LC (Ligand Centred) transitions in the UV region (250–340 nm) followed by weaker and very broad bands found within a wide spectral range (*ca.* 360 to 500 nm, Table 1, Fig. 2 and ESI S25–S36†) which might be confidently attributed to spin allowed ^{1}MLCT (Metal to Ligand Charge Transfer) processes involving the Ir(III) center and the two different types of aromatic ligands of the C^N cyclometalating and the N^N ancillary groups – that constitute its coordination sphere. The observed hypsochromic shift of ^{1}MLCT transitions can be confidently assigned to the switch from neutral to cationic species (Fig. 2). Upon excitation (λ_{exc} = 370 nm) of the corresponding dilute CH_3CN solutions, the neutral Ir(III) complexes exhibited bright luminescence, with typical ^{3}MLCT-shaped broad and structureless profiles centred in the region between λ_{max} = 532 and 590 nm (Table 1, ESI S25–S36†).[5] In all cases, the triplet character of the excited states was confirmed by the sensitivity to the presence of dissolved O_2 of both quantum yield (Φ) and lifetime values (τ, Table 1).

The analyses of the emission spectrum at 77 K evidenced, in some cases, the occurrence of structured profiles that might account for the interplay of ^{3}LC/^{3}MLCT type emissive excited states (Table 1, ESI S25–S36†).[5] The combination of 2-pyridyl tetrazolato (**PTZ$^-$**) and 2-pyrazinyl tetrazolato (**PYZ$^-$**) ligands with **[Ir(ppyCN)$_2$Cl]$_2$** and **[Ir(F$_2$ppy-CN)$_2$Cl]$_2$** dimers resulted in an unexpected emission behaviour exhibited by the resulting complexes.[9,10a–c] That is, when unsubstituted ppy and **F$_2$ppy** are used as cyclometalating ligands, **(PYZ)$^-$** – based Ir(III) complexes always displayed a significantly red shifted emission with respect to the **(PTZ)$^-$** ones.[9,10a–c] In contrast, the use of (**ppyCN**) and (**F$_2$ppy-CN**) as cyclometalating ligands turned in a reverse effect. For this new class of neutral compounds, **(PYZ)$^-$** derivatives have slightly blue shifted emissions (*ca.* 8 nm; λ_{max} = 582 nm for **[Ir(ppyCN)$_2$(PYZ)]**; 532 nm for **[Ir(F$_2$ppy-CN)$_2$(PYZ)]**) with respect to those observed for **(PTZ)$^-$** – based Ir(III) complexes (λ_{max} = 590 nm for **[Ir(ppyCN)$_2$(PTZ)]**; 540 nm for **[Ir(F$_2$ppy-CN)$_2$(PTZ)]**, Fig. 3 and Table 1). The introduction of a trifluoromethyl substituent (CF_3) in the backbone of the 5-aryl tetrazolato ligand **(PTZ-CF$_3$)$^-$** shifted the emission

This journal is © The Royal Society of Chemistry 2025

Open Access Article. Published on 13 May 2025. Downloaded on 7/11/2025 6:28:05 AM. This article is licensed under a Creative Commons Attribution-NonCommercial 3.0 Unported Licence.

Table 1 Selected photophysical data for neutral and cationic Ir(III) species reported in this work

Complex	Absorption	Emission[a,b] 298 K					Emission[c] 77 K	
CH_3CN as the solvent	λ (nm), $10^{-4}\varepsilon$ (cm^{-1} M^{-1})	λ_{em} (nm)	τ_{ox} (μs)	τ_{deox} (μs)	ϕ_{ox} (%)	ϕ_{deox} (%)	λ_{em} (nm)	τ (μs)
[Ir(ppyCN)$_2$(PYZ)]	266 (3.83), 330 (2.09), 410 (0.53), 470 (0.30)	582	0.08	0.96	2.1	23.0	532	3.30
[Ir(ppyCN)$_2$(PTZ-CF$_3$)]	263 (3.14), 329 (1.61), 418 (0.42), 464 *sh* (0.20)	584	0.07	0.74	2.2	12.2	542	5.57
[Ir(ppyCN)$_2$(PTZ)]	269 (3.94), 338 (1.84), 411 (0.54), 460 (0.30)	590	0.08	1.02	1.8	26.0	550	4.45
[Ir(F$_2$ppy-CN)$_2$(PYZ)]	255 (4.64), 321 (2.81), 385 (0.81), 470 *sh* (0.08)	532	0.18	1.06	6.2	16.0	490, 518	2.40
[Ir(F$_2$ppy-CN)$_2$(PTZ-CF$_3$)]	259 (5.25), 322 (2.51), 392 (0.64), 460 *sh* (0.20)	536	0.18	1.26	4.3	44.7	522	4.30
[Ir(F$_2$ppy-CN)$_2$(PTZ)]	262 (5.27), 330 (1.76), 382 (0.58), 450 *sh* (0.10)	540	0.12	1.4	5.0	21.0	524	4.20
[Ir(ppyCN)$_2$(PYZ-Me)]$^+$	270 (6.58), 323 (3.22), 402 (0.98), 460 *sh* (0.28)	614	0.08	0.43	1.0	7.13	548	3.51
[Ir(ppyCN)$_2$(PTZ-CF$_3$-Me)]$^+$	267 (2.39), 319 (1.00), 398 (0.24), 450 *sh* (0.38)	568	0.08	0.72	2.6	12.1	540	3.29
[Ir(ppyCN)$_2$(PTZ-Me)]$^+$	265 (6.18), 323 (3.30), 405 (0.70), 466 (0.40)	566	0.09	1.22	2.0	25.0	522	2.74
[Ir(F$_2$ppy-CN)$_2$(PYZ-Me)]$^+$	261 (5.40), 313 (2.99), 383 (0.79), 440 *sh* (0.38)	530	0.28	1.15	8.0	31.0	490, 520	2.48
[Ir(F$_2$ppy-CN)$_2$(PTZ-CF$_3$-Me)]$^+$	257 (3.53), 315 (1.79), 391 (0.56), 430 *sh* (0.32)	520	0.22	1.00	5.0	28.1	554	3.32
[Ir(F$_2$ppy-CN)$_2$(PTZ-Me)]$^+$	258 (6.14), 315 (3.14), 386 (0.94), 450 (0.25)	520	0.23	1.5	6.0	30.0	482, 514	2.34

[a] "Air" means air equilibrated solutions, "Ar" means deoxygenated solutions under an argon atmosphere; "sh" means shoulder. [b] $[Ru(bpy)_3]Cl_2/H_2O$ was used as a reference for quantum yield determination (Φ_r = 0.028).[13] [c] In frozen CH_3CN.

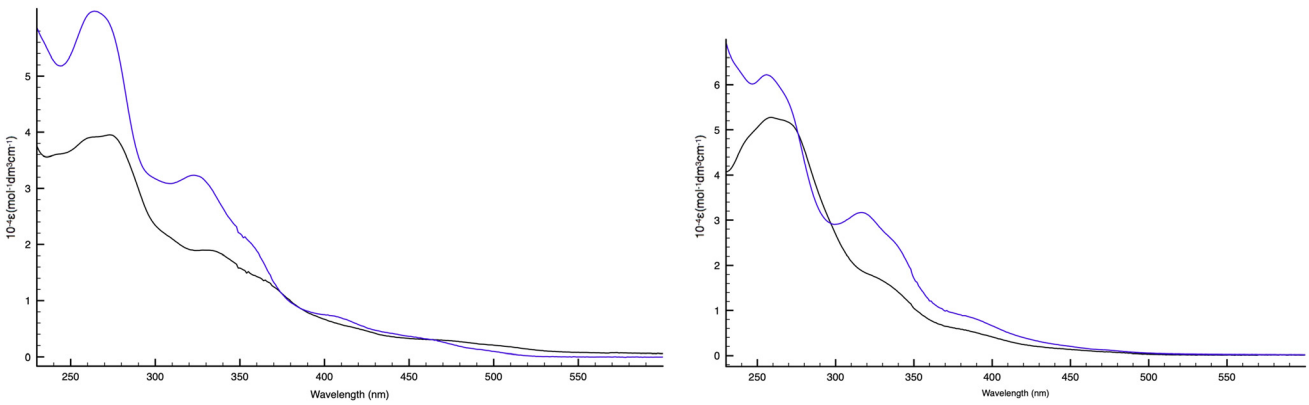

Fig. 2 Absorption profiles of (left) **[Ir(ppyCN)$_2$(PTZ)]** (black line) and **[Ir(ppyCN)$_2$(PTZ-Me)]$^+$** (blue line); (right) **[Ir(ppyCN)$_2$(PYZ)]** (black line) and **[Ir(ppyCN)$_2$(PYZ-Me)]$^+$** (blue line), 10^{-5} M, CH_3CN, 298 K.

maxima of the corresponding Ir(III) compounds in between **[Ir(C^N)$_2$(PYZ)]** and **[Ir(C^N)$_2$(PTZ)]** (Fig. 3 and Table 1).

As for neutral compounds, the photophysical properties of the corresponding cationic derivatives are, in some cases, rather different from the trend we expected. Indeed, the regioselective (N-3) addition of a methyl group to the metal coordinated tetrazolato ring of all the **Ir(ppy)$_2$**-and **Ir(F$_2$ppy)**-based complexes investigated so far, invariably resulted in the red shift of the emission maxima of the corresponding Ir(III)-tetrazole cationic complexes.[9,10a–c] This time, the conversion of **[Ir(C^N)$_2$(PTZ)]** and **[Ir(C^N)$_2$(PTZ-CF$_3$)]** into positively charged **[Ir(C^N)$_2$(PTZ-Me)]$^+$** and **[Ir(C^N)$_2$(PTZ-CF$_3$-Me)]$^+$**, produced a 20 to 24 nm blue shift of the emission maxima (Fig. 4) and a concomitant elongation of the of lifetime fitting decay (τ) (Table 1).

Conversely, the methylation of **[Ir(ppyCN)$_2$(PYZ)]** (λ_{max} = 582 nm, Fig. 5) resulted in the previously observed red shift of the emission maxima (**[Ir(ppyCN)$_2$(PYZ-Me)]$^+$** λ_{max} = 614 nm, Fig. 5), along with the reduction of both quantum yield (Φ) and lifetime values (Table 1).[5] Instead, the conversion of **[Ir(F$_2$ppy-CN)$_2$(PYZ)]** into **[Ir(F$_2$ppy-CN)$_2$(PYZ-Me)]$^+$** (Table 1 and Fig. 5) did not alter the emission maxima but increased both quantum yield (Φ) and lifetime values (Table 1).

Cyclic voltammetry

The electrochemical behavior of all the neutral and cationic Ir(III) species was investigated in CH_3CN solution by cyclic voltammetry (Table 2).

All the Ir(III) species displayed one irreversible process in the region of positive potentials, which is commonly ascribed

Open Access Article. Published on 13 May 2025. Downloaded on 7/11/2025 6:28:05 AM.
This article is licensed under a Creative Commons Attribution-NonCommercial 3.0 Unported Licence.

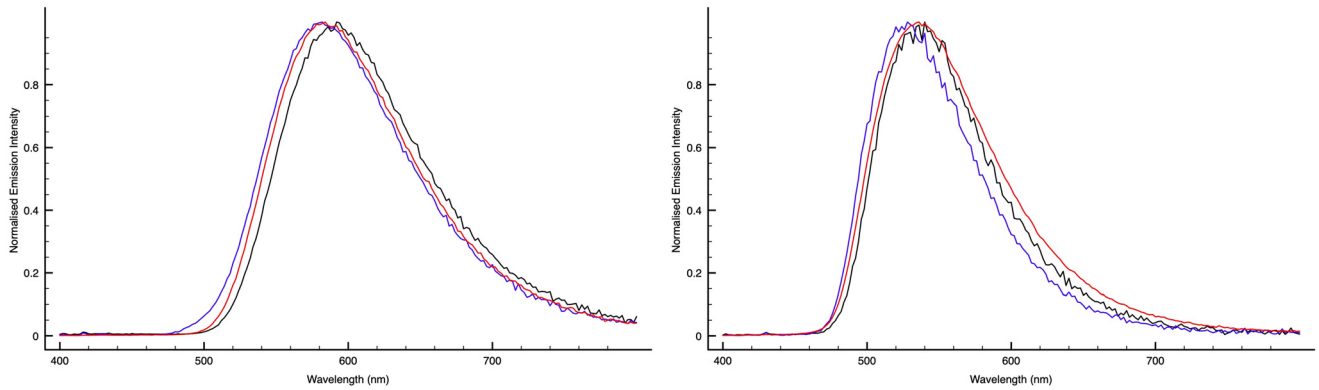

Fig. 3 (left) Normalized emission profiles of **[Ir(ppyCN)$_2$(PTZ)]** (black line), **[Ir(ppyCN)$_2$(PYZ)]** (blue line) and **[Ir(ppyCN)$_2$(PTZ-CF$_3$)]** (red line); (right) **[Ir(F$_2$ppy-CN)$_2$(PTZ)]** (black line), **[Ir(F$_2$ppy-CN)$_2$(PYZ)]** (blue line) and **[Ir(F$_2$ppy-CN)$_2$(PTZ-CF$_3$)]** (red line), 10^{-5} M CH_3CN, 298 K.

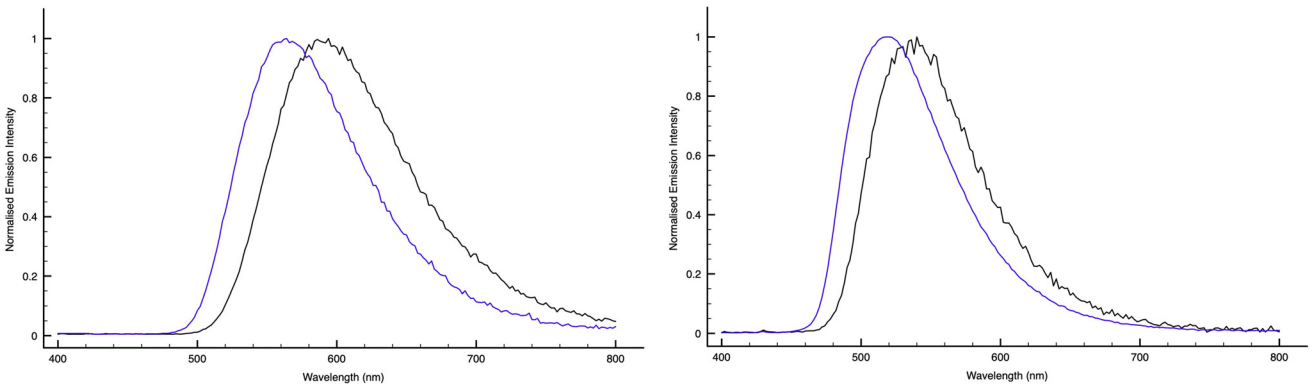

Fig. 4 (left) Normalised emission profiles of **[Ir(ppyCN)$_2$(PTZ)]** (black line) and **[Ir(ppyCN)$_2$(PTZ-Me)]$^+$** (blue line); (right) **[Ir(F$_2$ppy-CN)$_2$(PTZ)]** (black line) and **[Ir(F$_2$ppy-CN)$_2$(PTZ-Me)]$^+$** (blue line).

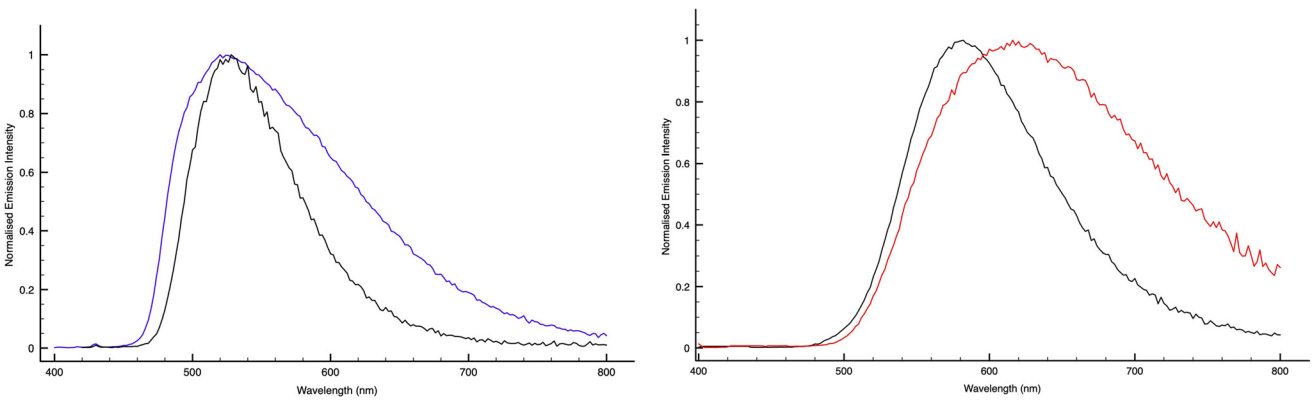

Fig. 5 (left) Normalised emission profiles of **[Ir(F$_2$ppy-CN)$_2$(PYZ)]** (black line) and **[Ir(F$_2$ppy-CN)$_2$(PYZ-Me)]$^+$** (blue line); (right) **[Ir(ppyCN)$_2$(PYZ)]** (black line) and **[Ir(ppyCN)$_2$(PYZ-Me)]$^+$** (red line).

to the formal oxidation of Ir(III) to Ir(IV). Along the series represented by **[Ir(ppyCN)$_2$(PYZ)]**, **[Ir(ppyCN)$_2$(PTZ)]** and **[Ir(ppyCN)$_2$(PTZ-CF$_3$)]**, this process gradually shifts towards more positive potentials (Table 2, ESI S37–S48†). Concerning the region of negative potentials, the first reductive process was observed at the same value for **[Ir(ppyCN)$_2$(PYZ)]** and **[Ir(ppyCN)$_2$(PTZ)]** (−1.34 V, Table 2, ESI S37–S48†), while for **[Ir(ppyCN)$_2$(PTZ-CF$_3$)]** the peak was observed at −1.26 V (Table 2, ESI S37–S48†). For the cationic compounds **[Ir(ppyCN)$_2$(PTZ-Me)]$^+$**, **[Ir(ppyCN)$_2$(PYZ-Me)]$^+$** and **[Ir(ppyCN)$_2$(PTZ-CF$_3$-Me)]$^+$**, a shift of the oxidation processes to more positive potentials was observed, with an extent of

This journal is © The Royal Society of Chemistry 2025

Open Access Article. Published on 13 May 2025. Downloaded on 7/11/2025 6:28:05 AM. This article is licensed under a Creative Commons Attribution-NonCommercial 3.0 Unported Licence.

Table 2 Half-wave ($E_{1/2}$) redox potentials[a] (*vs.* SCE) of neutral and cationic Ir(III) species at 25 °C in CH_3CN

Complex	Oxidation $E_{1/2}$ (V)	Reduction $E_{1/2}$ (V)		HOMO[c] exp. (eV)	LUMO[c] exp. (eV)	GAP[c] exp. (eV)	HOMO[d] calc. (eV)	LUMO[d] calc. (eV)	GAP[d] calc. (eV)	
[Ir(ppyCN)$_2$(PYZ)]	+1.37[b]	−1.34	−1.52	−5.77	−3.06	2.71	−5.92	−2.94	2.98	Gaussian
							−5.90	−2.80	3.10	ORCA
[Ir(ppyCN)$_2$(PTZ)]	+1.43[b]	−1.34	−1.55	−5.83	−3.05	2.78	−5.850	−2.90	2.95	Gaussian
							−5.8	−2.70	3.10	ORCA
[Ir(ppyCN)$_2$(PTZ-CF$_3$)]	+1.50[b]	−1.26	−1.46[b]	−5.90	−3.14	2.76	−5.90	−2.93	2.97	Gaussian
			−1.80[b]				−5.90	−2.80	3.10	ORCA
[Ir(ppyCN)$_2$(PYZ-Me)]$^+$	+1.49[b]	−1.04	−1.42	−5.89	−3.36	2.53	−6.17	−3.27	2.90	Gaussian
			−1.62				−6.20	−3.00	3.20	ORCA
[Ir(ppyCN)$_2$(PTZ-Me)]$^+$	+1.60[b]	−1.28	−1.47	−6.01	−3.12	2.89	−6.10	−3.04	3.07	Gaussian
							−6.10	−2.80	3.30	ORCA
[Ir(ppyCN)$_2$(PTZ-CF$_3$-Me)]$^+$	+1.59[b]	−1.16	−1.45[b]	−5.99	−3.24	2.75	−6.16	−3.22	2.94	Gaussian
			−1.67[b]				−6.00	−2.90	3.10	ORCA
[Ir(F$_2$ppy-CN)$_2$(PYZ)]	+1.36[b]	−1.25	−1.44	−5.76	−3.15	2.61	−6.31	−3.05	3.28	Gaussian
							−6.20	−2.90	3.30	ORCA
[Ir(F$_2$ppy-CN)$_2$(PTZ)]	+1.36[b]	−1.27	−1.47	−5.76	−3.13	2.63	−6.25	−3.00	3.24	Gaussian
							−6.20	−2.80	3.40	ORCA
[Ir(F$_2$ppy-CN)$_2$(PTZ-CF$_3$)]	+1.50[b]	−1.24	−1.43	−5.90	−3.16	2.74	−6.29	−3.03	3.27	Gaussian
							−6.20	−3.10	3.40	ORCA
[Ir(F$_2$ppy-CN)$_2$(PYZ-Me)]$^+$	+1.47[b]	−1.04	−1.37[b]	−5.87	−3.36	2.51	−6.58	−2.98	3.60	Gaussian
			−1.55[b]				−6.50	−3.10	3.40	ORCA
[Ir(F$_2$ppy-CN)$_2$(PTZ-Me)]$^+$	+1.85[b]	−1.26[b]	−1.57[b]	−6.25	−3.14	3.11	−6.51	−2.89	3.62	Gaussian
							−6.40	−3.00	3.40	ORCA
[Ir(F$_2$ppy-CN)$_2$(PTZ-CF$_3$-Me)]$^+$	+1.48[b]	−1.07	−1.36[b]	−5.88	−3.33	2.55	−6.56	−3.16	3.39	Gaussian
			−1.53[b]				−6.50	−2.90	3.60	ORCA

[a] In a 0.1 M $TBAPF_6/CH_3CN$ solution. [b] Irreversible process. [c] Calculated with $E_{HOMO} = -(E_{ox} + 4.4\ eV)$ and $E_{LUMO} = -(E_{red} + 4.4\ eV)$.[14] [d] See the DFT calculations section for further details.

+170, +120 and +90 mV with respect to their neutral counterparts (Table 2, ESI S37–S48†). The first reduction of **[Ir(ppyCN)$_2$(PTZ-CF$_3$-Me)]$^+$** falls at −1.16 V, a 290 mV displacement through less negative potentials with respect to its neutral precursor. The same trend was observed for **[Ir(ppyCN)$_2$(PYZ-Me)]$^+$**, with a reductive process at −1.04 V. Concerning **[Ir(ppyCN)$_2$(PTZ-Me)]$^+$**, the first reduction is centred at −1.28 V, thereby displaying a positive displacement of 60 mV if compared to its neutral analogue. The use of (**F$_2$ppy-CN**) as the (C^N) ligand did not substantially shift the potential value at which the oxidation of the neutral Ir(III) compounds occurred (Table 2), but has an impact on the region of negative potentials instead. The first reductive process of **[Ir(F$_2$ppy-CN)$_2$(PYZ)]** and **[Ir(F$_2$ppy-CN)$_2$(PTZ)]** underwent a positive offset of *ca.* 90 (Table 2) with respect to their (**ppyCN**) analogues. In the case of **[Ir(F$_2$ppy-CN)$_2$(PTZ-CF$_3$)]**, this value remains almost unchanged. The conversion of the **[Ir(F$_2$ppy-CN)$_2$]**-series into their cationic analogues produced the expected rise of their oxidation potentials toward more positive values, with the sole exception represented by **[Ir(F$_2$ppy-CN)$_2$(PTZ-CF$_3$-Me)]$^+$**, whose value is roughly identical to that observed from **[Ir(F$_2$ppy-CN)$_2$(PTZ-CF$_3$)]**. Concerning the reductions, for **[Ir(F$_2$ppy-CN)$_2$(PYZ-Me)]$^+$** and **[Ir(F$_2$ppy-CN)$_2$(PTZ-CF$_3$-Me)]$^+$** an appreciable shift through less negative values is observed. In contrast, the reduction potential of **[Ir(F$_2$ppy-CN)$_2$(PTZ-Me)]$^+$** is almost equivalent to that of **[Ir(F$_2$ppy-CN)$_2$(PTZ)]** (Table 2).

DFT calculations

To corroborate the experimental findings, DFT calculations were performed to compute the HOMO–LUMO gaps. Unlike photochemical experiments, where the electronic transitions can be assumed to be instantaneous *i.e.* the nuclei do not have time to relax, in the electrochemical experiments the oxidized and reduced molecules have ample time to undergo configurational rearrangements. Hence, we designed our computational experiments to mimic this process. One electron was added or removed for all neutral and cationic Ir(III) complexes and their geometry was allowed to fully relax. The self-consistent reaction field method was also used to partially include solvent effects. The electron affinity and ionization energies of the complexes were then used to compute the values of the HOMO–LUMO gap reported in Table 2 and the molecular orbitals shown in Fig. 6 (see the Experimental section for further details). The preponderant HOMO–LUMO composition for **[Ir(ppyCN)$_2$(PTZ)]**, and **[Ir(ppyCN)$_2$(PTZ-Me)]$^+$** consist of (Ir-phenyl) and (pyridine-CN), respectively. As the **PTZ$^-$/PTZ-Me** moiety is involved neither in the HOMO nor, in particular, in the composition of the LUMO, the observed blue shift of the emission profile from 590 to 566 nm can be confidently

Open Access Article. Published on 13 May 2025. Downloaded on 7/11/2025 6:28:05 AM.
This article is licensed under a Creative Commons Attribution-NonCommercial 3.0 Unported Licence.

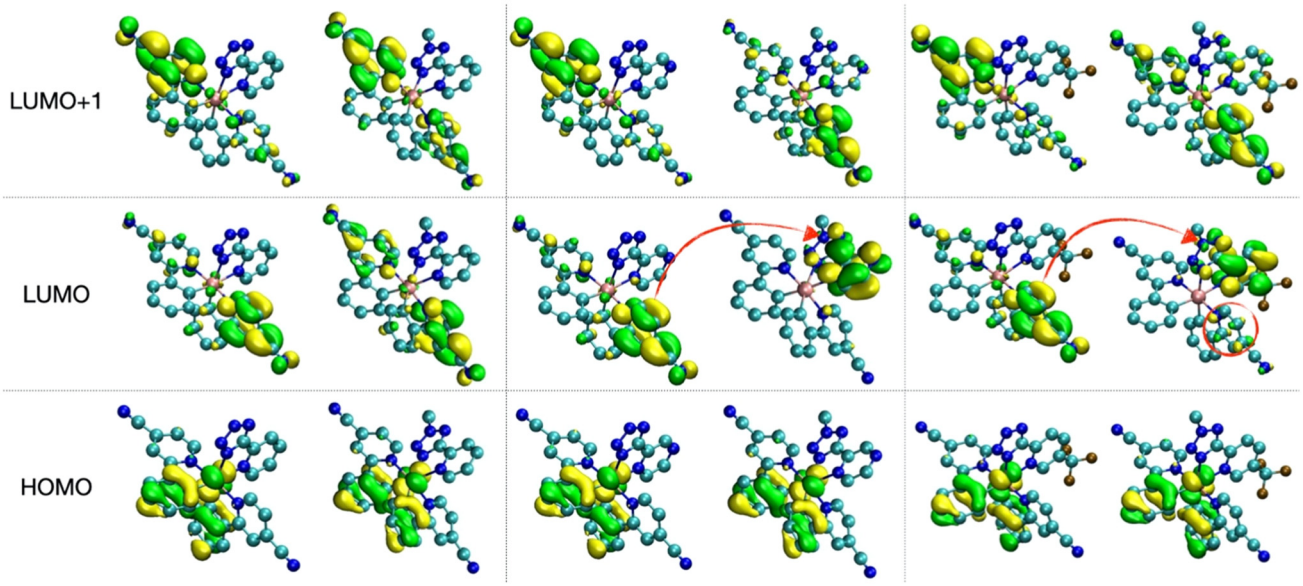

Fig. 6 Contour HOMO–LUMO for all the neutral and cationic fluorine-free Ir(III) complexes presented in this work; from left to right: **[Ir(ppyCN)$_2$(PTZ)]**, **[Ir(ppyCN)$_2$(PTZ-Me)]$^+$**, **[Ir(ppyCN)$_2$(PYZ)]**, **[Ir(ppyCN)$_2$(PYZ-Me)]$^+$**, **[Ir(ppyCN)$_2$(PTZ-CF$_3$)]**, and **[Ir(ppyCN)$_2$(PTZ-CF$_3$-Me)]$^+$** (see ESI Tables S2 and S3† and the experimental section for more details on DFT calculations; the images were produced using the Gaussian outputs, but the results are analogous to those obtained from ORCA).

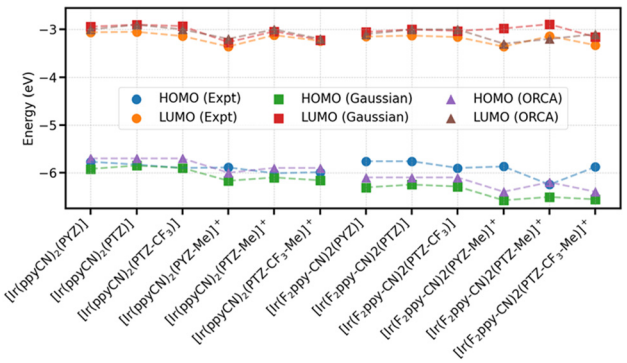

Fig. 7 Trend of HOMO/LUMO energies for the compounds studied in this work computed with Gaussian and ORCA.

ascribed to the stabilization of the HOMO that is induced by the formation of a positive net charge when the parent Ir(III)-tetrazolato complexes were converted into the corresponding cationic methylated derivatives. On the other hand, the presence of the **PYZ$^-$/PYZ-Me** ring together with the same Ir(ppyCN)-core, actually recall what was previously observed for Ir(III)-tetrazole based compounds.[9,10a–c] While the HOMO is still located on the (Ir-phenyl) portion for both **[Ir(ppyCN)$_2$(PYZ)]** and **[Ir(ppyCN)$_2$(PYZ-Me)]$^+$**, the LUMO level is composed of the (pyridine-CN) fragment for the neutral complex, and **PYZ-Me** for the cationic one. The concomitant lowering of the pyrazine – based LUMO energy explain the observed red shift to 614 nm of the emission profile of **[Ir(ppyCN)$_2$(PYZ-Me)]$^+$**, together with it being easier to reduce (−1.04 V, Table 2 and Fig. 7). With regards to **[Ir(ppyCN)$_2$(PTZ-CF$_3$)]** and **[Ir(ppyCN)$_2$(PTZ-CF$_3$-Me)]$^+$**, their HOMOs consist of the same (Ir-phenyl) portion as observed for the other examples. The LUMO level of **[Ir(ppyCN)$_2$(PTZ-CF$_3$)]** has a preponderant (pyridine-CN) composition, while its cationic analogue is mainly composed of the **PTZ-CF$_3$-Me** ligand, with a small contribution stemming from (pyridine-CN). This might account for the observed blue shift of the emission profile (from 584 to 536 nm) upon charge variation and for the observed electrochemical data (Table 2). These considerations can be extended also to the fluorinated derivatives, both neutral and cationic (Tables 1 and 2, Fig. 7, Fig. 8, ESI, Table S3†).

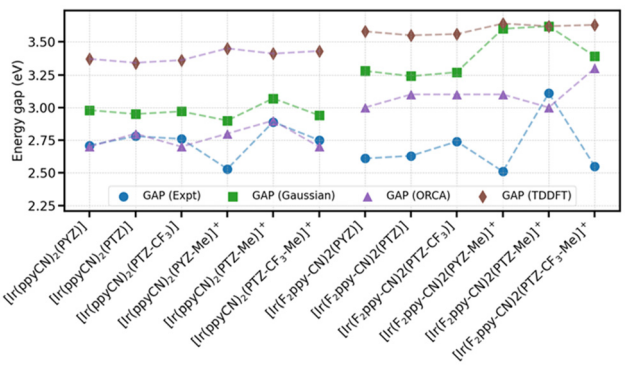

Fig. 8 Trend of HOMO–LUMO for the compounds studied in this work computed from the electron affinities and ionization energies obtained from Gaussian and ORCA. The TD-DFT gap was obtained from the ORCA calculations that used a larger basis set.

This journal is © The Royal Society of Chemistry 2025

Open Access Article. Published on 13 May 2025. Downloaded on 7/11/2025 6:28:05 AM.
This article is licensed under a Creative Commons Attribution-NonCommercial 3.0 Unported Licence.

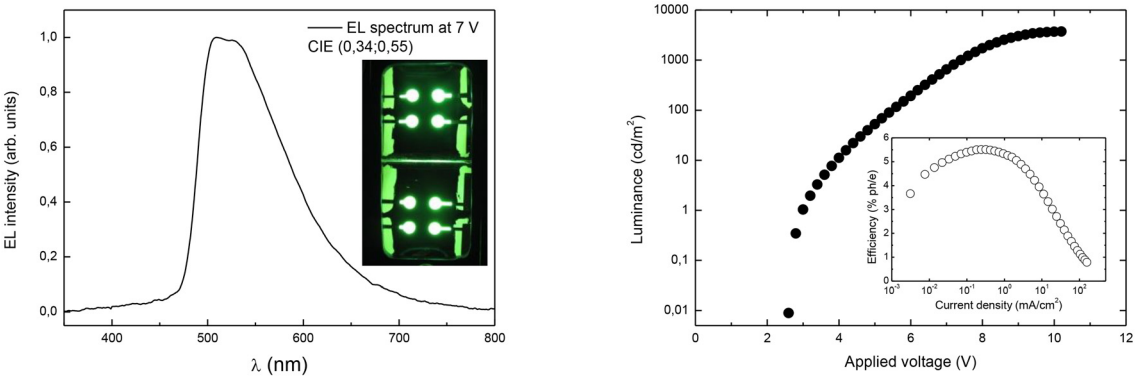

Fig. 9 (left) Electroluminescence spectra at 7 V of the OLED. In the inset is reported a photo of a green OLED; (right) luminance *vs.* applied voltage and external efficiency *vs.* current density (inset) of the OLED.

OLED device with [Ir(F$_2$ppy-CN)$_2$(PTZ)]

The acceptable solubility of the selected Ir(III) complex **[Ir(F$_2$ppy-CN)$_2$(PTZ)]** prompted us to study its application for the preparation of solution-processed OLEDs. This methodology is preferable due to its cost-effectiveness and in light of the recent insights about the inkjet print –OLED technology but, at the same time, it may suffer from several drawbacks that can limit the overall device efficiency.[15] The devices were fabricated by a combination of wet and dry processes (spin coating and sublimation in high vacuum) onto a pre-cleaned indium tin oxide (ITO) glass substrate (see the Experimental section). Holes were injected from the ITO anode and passed through a 40 nm thick transporting layer composed of PEDOT:PSS. Electrons were injected from an Al/LiF cathode and transported to the emitting layer (EML) through a 30 nm thick layer of 2,2′,2″-(1,3,5-benzinetriyl)-tris(1-phenyl-1-H-benzimidazole) (TPBi). Charges recombined in the 40 nm thick EML made of a 4,4′,4″-tris(*N*-carbazolyl-triphenylamine) (TCTA) matrix, hosting 8 wt% of **[Ir(F$_2$ppy-CN)$_2$(PTZ)]** as the emitter. The EL spectrum of the OLED and its related photo are shown in Fig. 9, left.

The OLED emission band is in the green region, and the corresponding CIE coordinates are (0.34, 0.55). The EL spectrum resembles the PL spectrum of the complex in solution media but it is slightly more structured due to rigid media (solid state). No significant contribution to the EL emission bands from the TBPi electron-transporting (hole-blocking) or TCTA binder layers is observed, indicating good charge carrier confinement within the EML and a complete energy transfer from the excited states of TCTA (generated by charge carrier recombination) to the Ir(III) complex. The luminance and external EL efficiency as a function of the applied voltage and current density of OLED is shown in Fig. 9, right. A maximum external EL efficiency of ≈5.5% with a luminance of ≈100 cd m^{-2} at about 5 V, and luminance of ≈1000 cd m^{-2} at about 7.5 V with an external EL efficiency ≈ 4% were obtained for the green OLED based on **[Ir(F$_2$ppy-CN)$_2$(PTZ)]**. The good OLED performances observed with **[Ir(F$_2$ppy-CN)$_2$(PTZ)]** as the emitter are generally comparable with those reported in the literature[15] and, importantly, appear in line with our past reports dealing with analogous devices where other Ir(III) tetrazolato complexes,[16] and tris carbonyl diimine Re(I) tetrazolato[17] derivatives were incorporated into OLEDs using the same high vacuum sublimation procedure described herein.

Conclusions

The class of Ir(III)-tetrazole-based complexes was further extended through chemical modifications of the cyclometalated phenylpyridine ligands (C^N), which were decorated with one (–CN) moiety at the –*para* position of the pyridyl ring. The effects of such structural variation upon conversion of the neutrally charged **[Ir(C^N)$_2$(N^N)]** (C^N = **ppyCN** or **F$_2$ppy-CN**, N^N = **PTZ$^-$**, **PYZ$^-$** or **PTZ-CF$_3$$^-$**) into the corresponding cationic **[Ir(C^N)$_2$(N^N)]$^+$**-type complexes were reflected at first on their photophysical behaviour, which appeared markedly different with respect to what was previously observed for fluorine and fluorine-free based ppy.[9,10a–c] Surprisingly, the regioselective addition of a methyl group at the N-3 position of the tetrazole ring produced a shift towards higher energies of the emissions stemming from **[Ir(C^N)$_2$(N^N)]** when (N^N) is represented by **PTZ$^-$** and **PTZ-CF$_3$$^-$** ($\Delta\lambda$ *ca.* 20–30 nm). In the case of **PYZ$^-$**, the conversion of the fluorine-free derivative into the cationic **[Ir(ppyCN)$_2$(PYZ-Me)]$^+$** produced the previously observed red shift of the emission profile ($\Delta\lambda$ *ca.* 20 nm), while it remained almost unchanged in the case of its (**F$_2$ppy-CN**)-based analogue. The outcome of the steady state emission spectra was further rationalized through electrochemical measurements (cyclic voltammetry) and TDDFT calculations to highlight how the emission output of this new class of Ir(III) complexes is mainly regulated by the nature of the cyclometalated ligand (C^N). More precisely, while the HOMO level is invariably composed of the (Ir-phenyl) or (Ir-F$_2$ phenyl) fragment, the lowest unoccupied molecular orbital is located on the (pyridine-CN) portion. The sole exception is represented by **[Ir(ppyCN)$_2$(PYZ-Me)]$^+$**, in which the LUMO is composed of the tetrazole ligand **PYZ-Me**. The possibility of a straightforward

Open Access Article. Published on 13 May 2025. Downloaded on 7/11/2025 6:28:05 AM.
This article is licensed under a Creative Commons Attribution-NonCommercial 3.0 Unported Licence.

fine colour tuning to both lower and higher energies of such kinds of molecules becomes relevant in the field of solid state lighting, where usually Ir(III) cyclometalates are used as phosphorescent materials in the fabrication of OLED and LEEC devices. In this context, the green **[Ir(F$_2$ppy-CN)$_2$(PTZ)]** emitter was finally tested for the preparation of solution-processed OLEDs, returning performances in line with those reported for similar compounds.

Experimental section

General considerations

All the reagents and solvents were obtained commercially (Sigma Aldrich/Merck, Alfa Aesar, Strem Chemicals) and used as received without any further purification, unless otherwise specified. When required, reactions were carried out under an argon atmosphere following standard Schlenk protocols. The purification of the Ir(III) complexes was performed *via* column chromatography with the use of Al_2O_3 (Brockmann grade I or II) as the stationary phase. ESI-mass spectra were recorded using a Waters ZQ-4000 instrument (for ESI-MS, acetonitrile was used as the solvent). Nuclear magnetic resonance spectra (^{1}H and ^{13}C) were always recorded using a Varian Mercury Plus 400 (^{1}H, 399.9; ^{13}C, 101.0 MHz). ^{1}H and ^{13}C chemical shifts were referenced to residual solvent resonances (^{1}H/^{13}C: acetone-d^6 2.05/29.84 ppm; CD_3CN 1.94/118.26 ppm; DMSO-d^6 2.49/39.52 ppm; $CDCl_3$ 7.26/77.16 ppm).

Photophysics

Absorption spectra were recorded at room temperature using an Agilent Cary 100 UV-vis spectrometer. Uncorrected steady-state emission and excitation spectra were recorded on an Edinburgh FLSP920 spectrometer equipped with a 450 W xenon arc lamp, double excitation and single emission monochromators, and a Peltier-cooled Hamamatsu R928P photomultiplier tube (185–850 nm). Emission and excitation spectra were acquired with a cut-off filter (395 nm) and corrected for source intensity (lamp and grating) and emission spectral response (detector and grating) by a calibration curve supplied with the instrument. The wavelengths for the emission and excitation spectra were determined using the absorption maxima of the MLCT transition bands (emission spectra) and at the maxima of the emission bands (excitation spectra). Quantum yields (Φ) were determined using the optically dilute method of Crosby and Demas[18] at the excitation wavelength obtained from absorption spectra on a wavelength scale [nm] and compared to the reference emitter ($[Ru(bpy)_3]^{2+}$ in H_2O) using the following equation:[19]

$$\Phi_s = \Phi_r \left[\frac{A_r(\lambda_r)}{A_s(\lambda_s)}\right]\left[\frac{I_r(\lambda_r)}{I_s(\lambda_s)}\right]\left[\frac{n_s{}^2}{n_r{}^2}\right]\left[\frac{D_s}{D_r}\right]$$

where A is the absorbance at the excitation wavelength (λ), I is the intensity of the excitation light at the excitation wavelength (λ), n is the refractive index of the solvent, D is the integrated intensity of the luminescence, and Φ is the quantum yield. The subscripts r and s refer to the reference and the sample, respectively. A stock solution with an absorbance > 0.1 was prepared, then a 10 times diluted solution was obtained, resulting in an absorbance of about 0.07/0.08 depending on the sample considered. The Lambert–Beer law was assumed to remain linear at the concentrations of the solutions. The degassed measurements were obtained after the solutions were bubbled for 10 minutes under an Ar atmosphere, using a septa-sealed quartz cell. Air-equilibrated $[Ru(bpy)_3]Cl_2/H_2O$ solution (Φ = 0.028)[13] was used as the reference. The quantum yield determinations were performed at identical excitation wavelengths for the sample and the reference, therefore deleting the $I(\lambda_r)/I(\lambda_s)$ term in the equation. Emission lifetimes (τ) were determined with the single photon counting technique (TCSPC) with the same Edinburgh FLSP920 spectrometer using pulsed picosecond LED (EPLED 360, FWHM < 800 ps) as the excitation source, with repetition rates between 1 kHz and 1 MHz, and the above-mentioned R928P PMT as the detector. The goodness of fit was assessed by minimizing the reduced χ^2 function and by visual inspection of the weighted residuals. To record the 77 K luminescence spectra, the samples were put in quartz tubes (2 mm diameter) and inserted in a special quartz Dewar filled with liquid nitrogen. The solvent used in the preparation of the solutions for the photophysical investigations was of spectrometric grade. Experimental uncertainties were estimated to be ±8% for lifetime determinations, ±20% for quantum yields, and ±2 nm and ±5 nm for absorption and emission peaks, respectively.

Cyclic voltammetry

$TBAPF_6$ (tetrabutylammonium hexafluorophosphate, Sigma Aldrich) was used as received as the supporting electrolyte, and CH_3CN was distilled over CaH_2 and thoroughly degassed under N_2 before each measurement. Electrochemical experiments were recorded with a Metrohm Autolab PGSTAT302N potentiostat–galvanostat using a calomel electrode as the reference (303/SCG/6 – Amel Electrochemistry) and a platinum solid electrode (492/Pt/2 – Amel Electrochemistry) as the working electrode.

Ligand synthesis

Tetrazole derivatives are nitrogen rich molecules that can be used as components for explosive mixtures.[20] The reactions described herein were only run on a few grams scale and no problems were encountered. However, *great caution* should be exercised when handling or heating compounds of this type. Following the general method reported by Koguro and co-workers,[21] tetrazole ligands [H-**PTZ**], [H-**PYZ**], and [H-**PTZ-CF$_3$**] were obtained in an almost quantitative yield. [H-**PTZ**] **^{1}H-NMR** (DMSO-d^6, 400 MHz) δ (ppm) = 8.82 (m, 1H), 8.25 (m, 1H), 8.10 (m, 1H), 7.66 (m, 1H). **^{13}C-NMR**, (DMSO-d^6, 100 MHz) δ (ppm) = 155.3, 150.5, 144.1, 138.7, 126.6, 123.1. [H-**PYZ**] **^{1}H-NMR** (DMSO-d^6, 400 MHz) δ (ppm) = 9.42 (d, J_{H-H} = 1.2 Hz, 1H), 8.89 (m, 2H). **^{13}C-NMR**, (DMSO-d^6, 100 MHz) δ (ppm) = 165.1, 147.7, 145.6, 144.6, 143.9. [H-**PTZ-CF$_3$**] (DMSO-d^6, 400 MHz) δ (ppm) = 8.56 (m, 1H), 8.32 (m, 1H), 8.10 (m,

 This journal is © The Royal Society of Chemistry 2025

Open Access Article. Published on 13 May 2025. Downloaded on 7/11/2025 6:28:05 AM. This article is licensed under a Creative Commons Attribution-NonCommercial 3.0 Unported Licence.

1H), 7.75 (m, 1H). **^{13}C-NMR**, (DMSO-d^6, 100 MHz) δ (ppm) = 163.2, 152.1, 149.9, 136.8, 126.3, 124.7, 123.1.

(**ppyCN**) and (**F$_2$ppy-CN**) were obtained by standard Suzuki–Miyaura coupling reactions between 4-cyano 2-bromopyridine and phenylboronic acid or 2,4-difluorophenyl boronic acid in the presence of [Pd(pph$_3$)$_4$]. (**ppyCN**) **^{1}H-NMR**, ($CDCl_3$, 400 MHz) δ (ppm) = 8.82 (d, J_{HH} = 4.4 Hz, 1H), 7.97 (m, 2H), 7.90 (s, 1H), 7.48 (m, 3H), 7.41 (m, 1H). Y = 0.339 g (86%). (**F$_2$ppy-CN**) **^{1}H-NMR**, ($CDCl_3$, 400 MHz) δ (ppm) = 8.88 (d, J_{HH} = 4.8 Hz, 1H), 8.08 (m, 1H), 8.02 (m, 1H), 7.48 (d, J_{HH} = 5.2 Hz, 1H), 7.04 (m, 1H), 6.96 (m, 1H). **^{19}F-NMR** ($CDCl_3$, 376 MHz) δ (ppm) = −106.69, −112.11. Y = 0.391 g (83%).

Dichlorobridged Ir(III) dimer **[Ir(ppyCN)$_2$Cl]$_2$** was obtained according to the Nonoyama protocol;[12] for **[Ir(F$_2$ppy-CN)$_2$Cl]$_2$**, the reaction was carried out over a period of 48 h in pure ethoxyethanol.

General procedure for the synthesis of neutral [Ir(C^N)$_2$(N^N)]-type complexes

To a 3 : 1 solution of DCM/EtOH (15 + 5 mL), the desired dichloro-bridged Ir(III) dimer **[Ir(C^N)$_2$Cl]$_2$** (1 eq.) and 2.5 eq. of [H-**PTZ**], [H-**PYZ**] or [H-**PTZ-CF$_3$**] were added. The solution was stirred at r.t. for 6 h. The solvent was removed by rotary evaporation and the crude was subsequently purified with Al_2O_3 column chromatography eluted with a 40 : 1 DCM/CH_3OH or DCM/acetone gradient from 8 : 2 to 6 : 4 mixtures, yielding the desired neutral Ir(III) complex as the second fraction.

[Ir(ppyCN)$_2$(PTZ)] **^{1}H-NMR** (CD_3CN, 400 MHz). δ (ppm) = 8.66–8.58 (m, 2H), 8.39–8.36 (m, 1H), 8.20–8.16 (m, 1H), 8.05–8.01 (m, 2H), 7.96–7.94 (m, 1H), 7.83–7.81 (m, 2H), 7.52–7.47 (m, 2H), 7.39–7.37 (m, 1H), 7.09–7.05 (m, 1H), 6.99–6.95 (m, 2H), 6.88–6.84 (m, 1H), 6.48–6.45 (m, 1H), 6.38–6.36 (m, 1H). **^{13}C-NMR** (acetone-d^6, 100 MHz) δ (ppm) = 170.20, 170.01, 165.34 (Ct), 153.32, 151.12, 150.83, 150.70, 149.87, 148.88, 143.61, 143.00, 140.54, 132.56, 132.37, 131.86, 131.06, 127.08, 126.48, 126.03, 125.48, 124.95, 123.17, 122.49, 122.45, 122.28, 122.16, 121.85, 116.32, 104.20. **ESI-MS** (m/z, CH_3CN): [M + H$^+$] = 698; [M + Na$^+$] = 720. Y = 0.090 g (51%). Anal. calcd for $C_{30}H_{18}N_9Ir_1$ (696.74) C 51.72, H 2.61, N 18.09. Found: C 49.63, H 2.46, N 17.08.

[Ir(ppyCN)$_2$(PYZ)] **^{1}H-NMR** (acetone-d^6, 400 MHz). δ (ppm) = 9.54 (d, J_{H-H} = 1.2 Hz, 1H), 8.68 (d, J_{H-H} = 3.2 Hz, 1H), 8.59 (m, 2H), 8.20 (d, J_{H-H} = 6 Hz, 1H), 8.03 (d, J_{H-H} = 8.0 Hz, 1H), 7.94 (d, J_{H-H} = 8.0 Hz, 1H), 7.85 (d, J_{H-H} = 3.2 Hz, 1H), 7.80 (d, J_{H-H} = 6.0 Hz, 1H), 7.49 (d, J_{H-H} = 6.0 Hz, 1H), 7.35 (d, J_{H-H} = 6.0 Hz, 1H), 7.08 (m, 1H), 7.00 (m, 1H), 6.94 (m, 1H), 6.87 (m, 1H), 6.47 (d, J_{H-H} = 7.6 Hz, 1H), 6.36 (d, J_{H-H} = 7.6 Hz, 1H). **^{13}C-NMR** (CD_3CN, 100 MHz). δ (ppm) = 169.40, 169.24, 162.82 (Ct), 151.36, 151.11, 151.00, 148.53, 147.89, 144.80, 144.67, 144.36, 143.62, 142.90, 132.50, 132.20, 131.96, 131.32, 126.35, 125.99, 125.79, 125.23, 123.72, 123.08, 122.90, 122.82, 122.25, 122.14. **ESI-MS** (m/z, CH_3CN): [M + Na$^+$] = 721; [M + K$^+$] = 737. Y = 0.101 g (57%). Anal. calcd for $C_{29}H_{17}N_{10}Ir_1$ (697.73) C 49.92, H 2.46, N 20.07. Found: C 49.87, H 2.44, N 20.05.

[Ir(ppyCN)$_2$(PTZ-CF$_3$)] **^{1}H-NMR** (acetone-d^6, 400 MHz). δ (ppm) = 8.62–8.48 (m, 3H), 8.51–8.48 (m, 1H), 8.24–8.22 (m, 1H), 8.06–8.04 (m, 2H), 7.97–7.94 (m, 1H), 7.84–7.82 (m, 1H), 7.51–7.49 (m, 1H), 7.35–7.33 (m, 1H), 7.12–7.08 (m, 1H), 7.04–6.99 (m, 1H), 6.97–6.94 (m, 1H), 6.89–6.85 (m, 1H), 6.52–6.50 (m, 1H), 6.38–6.36 (m, 1H). **^{13}C-NMR** (acetone-d^6, 100 MHz). δ (ppm) = 169.34, 169.28, 163.1 (Ct), 152.8, 151.6, 150.8, 150.7, 147.05, 146.99, 146.95, 143.22, 142.43, 137.47, 137.44, 132.12, 131.67, 131.41, 130.57, 128.09, 127.75, 126.03, 125.99, 125.81, 125.56, 125.51, 125.44, 125.11, 124.45, 124.37, 123.91, 122.98, 122.92, 122.89, 122.83, 122.79, 122.13, 122.08, 122.04, 121.98, 121.82, 121.79, 121.73, 121.48, 121.23, 118.62, 118.40, 115.75, 115.73. **ESI-MS** (m/z, CH_3CN): [M + CH_3CN] = 806; Y = 0.137 g (95%). Anal. calcd for $C_{31}H_{17}N_9F_3Ir_1$ (764.74) C 48.68, H 2.24, N 16.48. Found: C 49.19, H 2.50, N 17.38.

[Ir(F$_2$ppy-CN)$_2$(PTZ)] **^{1}H-NMR** (CD_3CN, 400 MHz). δ (ppm) = 8.51–8.48 (m, 2H), 8.37–8.34 (m, 1H), 8.11–8.07 (m, 1H), 7.81–7.78 (m, 2H), 7.71–7.69 (m, 1H), 7.41–7.37 (m, 1H), 7.30–7.26 (m, 2H), 6.77–6.66 (m, 2H), 5.92–5.89 (m, 1H), 5.84–5.81 (m, 1H). **^{13}C-NMR** (acetone-d^6, 100 MHz) δ (ppm) = 166.25, 166.21, 166.16, 165.40, 164.53, 163.78, 157.83, 153.15, 153.10, 151.78, 151.61, 151.59, 149.67, 141.49, 128.09, 127.94, 127.84, 126.64, 126.20, 126.11, 125.97, 125.89, 125.75, 123.82, 123.72, 123.55, 123.36, 116.49, 116.47, 115.42, 115.31, 115.06, 114.95, 99.97, 99.79, 99.61, 99.32, 99.14, 98.96. **^{19}F-NMR** (CD_3CN, 376 MHz) δ (ppm) = −106.24, −107.07, −108.69, −109.59. **ESI-MS** (m/z, CH_3CN): [M + H$^+$] = 769; [M + Na$^+$] = 790. Y = 0.110 g (63%). Anal. calcd for $C_{30}H_{14}N_9F_4Ir_1$ (768.7) C 46.88, H 1.84, N 16.4. Found: C 45.2, H 2.05, N 16.02.

[Ir(F$_2$ppy-CN)$_2$(PYZ)] **^{1}H-NMR** (acetone-d^6, 400 MHz). δ (ppm) = 9.53 (s, 1H), 8.72–8.71 (m, 1H), 8.59–8.58 (m, 1H), 8.29–8.27 (m, 1H), 8.04–8.03 (m, 1H), 7.81–7.80 (m, 1H), 7.62–7.60 (m, 1H), 7.47–7.45 (m, 1H), 7.23–7.15 (m, 1H), 6.85–6.71 (m, 2H), 6.05–6.02 (m, 1H), 5.88–5.86 (m, 1H). **^{13}C-NMR** (acetone-d^6, 100 MHz) δ (ppm) = 166.61, 166.48, 165.94, 162.43, 162.30, 161.87, 160.74, 160.61, 160.32, 160.19, 155.28, 155.21, 151.21, 151.17, 150.40, 148.25, 144.39, 144.21, 143.52, 128.84, 128.11, 125.89, 125.32, 125.20, 125.11, 124.90, 122.85, 122.68, 115.51, 115.50, 114.70, 114.67, 114.52, 114.50, 114.09, 114.06, 113.91, 113.89, 99.48, 99.21, 98.94, 98.76, 98.49, 98.22. **^{19}F-NMR** (acetone-d^6, 376 MHz) δ (ppm) = −105.62, −106.64, −108.58, −109.71. **ESI-MS** (m/z, CH_3CN): [M] = 769; [M + Na$^+$] = 791. Y = 0.123 g (70%). Anal. calcd for $C_{29}H_{13}N_{10}F_4Ir_1$ (769.69) C 45.26, H 1.7, N 18.2. Found: C 45.10, H 1.54, N 17.95.

[Ir(F$_2$ppyCN)$_2$(PTZ-CF$_3$)] **^{1}H-NMR** (acetone-d^6, 400 MHz). δ (ppm) = 8.47–8.42 (m, 3H), 8.19–8.18 (m, 1H), 8.03 (m, 1H), 7.69–7.67 (m, 1H), 7.50–7.48 (m, 1H), 7.32–7.30 (m, 2H), 6.75–6.59 (m, 2H), 5.97–5.94 (m, 1H), 5.74–5.71 (m, 1H). **^{13}C-NMR** (acetone-d^6, 100 MHz) δ (ppm) = 166.14, 166.09, 165.96, 165.91, 165.42, 165.34, 164.45, 164.37, 163.81, 163.72, 163.64, 163.33, 163.24, 162.07, 161.99, 161.61, 161.52, 156.68, 156.64, 153.19, 152.23, 152.04, 151.96, 151.74, 151.61, 151.56, 148.38, 148.35, 148.32, 139.07, 139.05, 129.28, 129.06, 128.29, 127.74, 126.77, 126.34, 126.19, 125.90, 125.76, 124.24, 124.10, 124.02, 123.67, 123.58, 123.52, 122.44, 116.43, 115.73, 115.71,

Open Access Article. Published on 13 May 2025. Downloaded on 7/11/2025 6:28:05 AM. This article is licensed under a Creative Commons Attribution-NonCommercial 3.0 Unported Licence.

115.61, 115.59, 114.97, 114.95, 114.85, 114.83, 102.51, 100.26, 100.08, 99.90, 99.56, 99.38, 99.20. **^{19}F-NMR** (acetone-d^6, 376 MHz) δ (ppm) = −63.48, −105.54, −105.56, −106.65, −106.67, −108.50, −108.51, −109.71, −109.71. **ESI-MS** (m/z, CH_3CN): $[M + Na^+]$ = 860; $[M + CH_3CN]$ = 878. Y = 0.09 g (85%). Anal. calcd for $C_{31}H_{13}N_9F_7Ir_1$ (836.7) C 44.5, H 1.57, N 15.07. Found: C 41.7, H 1.64, N 13.68.

General procedure for the synthesis of cationic [Ir(C^N)$_2$(N^N)]$^+$[PF$_6$]$^-$-type complexes

1 eq. of the desired neutral Ir(III) complex was added to dichloromethane (15 mL) and the mixture was allowed to cool down to −50 °C by immersion into an ethanol/liquid nitrogen cold bath. Then, methyl trifluoromethanesulfonate (1.2 eq.) was added. The reaction was stirred under nitrogen for 30 minutes while being kept in a cold bath and then allowed to warm up to room temperature and stirred for 3 hours. Anion exchange was carried out by adding an excess of NH_4PF_6 to the solution and stirring for 30 minutes. The product was then extracted with H_2O (3 × 10 mL) and the organic components were combined and dried over anhydrous $MgSO_4$. Subsequent purification by column chromatography on Al_2O_3 eluted with a CH_2Cl_2/acetone 6 : 4 yielded the desired cationic Ir(III) complex as the second fraction.

[Ir(ppyCN)$_2$(PTZ-Me)]$^+$[PF$_6$]$^-$ **^{1}H-NMR** (acetone-d^6, 400 MHz). δ (ppm) = 8.69–8.68 (m, 2H), 8.63–8.61 (m, 1H), 8.42–8.37 (m, 2H), 8.36–8.15 (m, 1H), 8.08–8.01 (m, 3H), 7.84–7.80 (m, 1H), 7.47–7.43 (m, 2H), 7.15–7.08 (m, 1H), 7.07–6.99 (m, 2H), 6.97–6.43 (m, 1H), 6.43–6.39 (m, 2H), 4.54 (s, 3H). **^{13}C-NMR** (acetone-d^6, 100 MHz) δ (ppm) = 170.13, 169.59, 167.76 (C_t), 153.22, 153.06, 152.67, 149.67, 146.43, 146.28, 144.44, 144.34, 142.72, 133.69, 133.29, 133.19, 132.64, 131.69, 127.84, 127.40, 126.77, 126.64, 126.53, 125.11, 124.70, 124.15, 124.07, 123.96, 123.86, 117.23, 117.20, 42.47 (CH_3). **ESI-MS** (m/z, CH_3CN): $[M]^+$ = 712; $[M]^-$ = 145. Y = 0.036 g (70%). Anal. calcd for $C_{31}H_{21}N_9F_6P_1Ir_1$ (856.74) C 43.46, H 2.47, N 14.71. Found: C 43.59, H 2.51, N 14.89.

[Ir(ppyCN)$_2$(PYZ-Me)]$^+$[PF$_6$]$^-$ **^{1}H-NMR** (acetone-d^6, 400 MHz). δ (ppm) = 9.77 (m, 1H), 8.69 (m, 2H), 8.34–8.31 (m, 2H), 8.09–8.03 (m, 3H), 7.45–7.43 (m, 3H), 7.17–6.94 (m, 4H), 6.44–6.39 (m, 1H), 6.38–6.37 (m, 1H), 4.59 (s, 3H). **^{13}C-NMR** (acetone-d^6, 100 MHz) δ (ppm) = 169.82, 169.43, 166.26 (C_t), 151.72, 151.60, 151.51, 146.54, 145.40, 145.33, 144.17, 142.79, 142.62, 139.80, 131.85, 131.68, 131.58, 131.08, 126.20, 125.79, 125.23, 124.98, 123.77, 123.29, 122.59, 122.51, 122.30, 115.49, 42.69 (CH_3). **ESI-MS** (m/z, CH_3CN): $[M]^+$ = 713; $[M]^-$ = 145. Y = 0.042 g (64%). Anal. calcd for $C_{30}H_{20}N_{10}F_6P_1Ir_1$ (857.73) C 42.01, H 2.35, N 16.33. Found: C 42.47, H 2.43, N 16.50.

[Ir(ppyCN)$_2$(PTZ-CF$_3$-Me)]$^+$[PF$_6$]$^-$ **^{1}H-NMR** (acetone-d^6, 400 MHz). δ (ppm) = 8.86–8.85 (m, 1H), 8.73–8.67 (m, 3H), 8.39–8.37 (m, 1H), 8.33–8.31 (m, 1H), 8.22–8.21 (m, 1H), 8.11–8.09 (m, 1H), 8.05–8.03 (m, 1H), 7.45–7.40 (m, 2H), 7.19–7.15 (m, 1H), 7.10–7.04 (m, 3H), 6.99–6.94 (m, 1H), 6.49–6.47 (m, 1H), 6.40–6.38 (m, 1H), 4.56 (s, 3H). **^{13}C-NMR** (acetone-d^6, 100 MHz) δ (ppm) = 169.04, 168.55, 165.96 (Ct), 151.59, 151.37, 148.25, 148.00, 147.12, 143.66, 142.91, 142.75, 138.78, 131.90, 131.65, 131.22, 126.22, 125.78, 125.28, 124.99, 123.78, 123.22, 122.61, 122.49, 122.41, 122.19, 115.55, 68.82, 67.76, 65.96, 65.37, 54.59, 41.79. **ESI-MS** (m/z, CH_3CN): $[M]^+$ = 780; $[M]^-$ = 145. Y = 0.113 g (87%). Anal. calcd for $C_{32}H_{20}N_9F_9P_1Ir_1$ (924.74) C 41.56, H 2.18, N 13.63. Found: C 42.2, H 2.41, N 13.03.

[Ir(F$_2$ppy-CN)$_2$(PTZ-Me)]$^+$[PF$_6$]$^-$ **^{1}H-NMR** (acetone-d^6, 400 MHz). δ (ppm) = 8.67–8.63 (m, 2H), 8.47–8.41 (m, 2H), 8.40–8.20 (m, 2H), 7.88–7.84 (m, 1H), 7.57–7.53 (m, 2H), 6.92–6.81 (m, 3H), 5.99–5.93 (m, 2H), 4.56 (s, 3H). **^{13}C-NMR** (acetone-d^6, 100 MHz) δ (ppm) = 170.19, 169.91, 168.50 (C_t), 153.06, 152.60, 152.45, 145.09, 142.52, 131.35, 126.78, 126.06, 124.30, 124.24, 116.27, 100.94, 100.67, 100.57, 42.67 (CH_3). **^{19}F-NMR** (acetone-d^6, 376 MHz) δ (ppm) = −72.03, −73.91, −105.34, −106.09, −108.04, −108.76. **ESI-MS** (m/z, CH_3CN): $[M]^+$ = 784; $[M]^-$ = 145. Y = 0.041 g (58%). Anal. calcd for $C_{31}H_{17}N_9F_{10}P_1Ir_1$ (928.7) C 40.09, H 1.85, N 13.57. Found: C 40.12, H 1.98, N 13.55.

[Ir(F$_2$ppy-CN)$_2$(PYZ-Me)]$^+$[PF$_6$]$^-$ **^{1}H-NMR** (CD_3CN, 400 MHz). δ (ppm) = 9.64 (m, 1H), 8.86 (m, 1H), 8.55 (m, 1H), 7.98–7.94 (m, 2H), 7.84 (m, 1H), 7.42–7.38 (m, 2H), 6.80 (m, 3H), 5.85 (m, 1H), 5.78 (m, 1H), 4.48 (s, 3H). **^{13}C-NMR** (acetone-d^6, 100 MHz) δ (ppm) = 169.94, 169.51, 166.89 (C_t), 152.02, 151.98, 151.96, 150.03, 149.95, 147.65, 147.58, 145.79, 145.59, 139.25, 126.03, 125.88, 125.80, 125.60, 125.49, 125.28, 123.54, 123.52, 115.29, 100.34, 100.07, 99.87, 99.80, 99.60, 99.34, 67.71, 65.97, 65.57, 41.96 (CH_3). **^{19}F-NMR** (CD_3CN, 376 MHz) δ (ppm) = −72.03, −73.91, −105.06, −105.78, −107.78, −108.54. **ESI-MS** (m/z): $[M^+]$ = 785; $[M^-]$ = 145. Y = 0.031 g (50%). Anal. calcd for $C_{30}H_{16}N_{10}F_{10}P_1Ir_1$ (929.69) C 38.76, H 1.73, N 15.07. Found: C 38.83, H 1.82, N 15.11.

[Ir(F$_2$ppyCN)$_2$(PTZ-CF$_3$-Me)]$^+$[PF$_6$]$^-$ **^{1}H-NMR** (acetone-d^6, 400 MHz). δ (ppm) = 8.62–8.55 (m, 4H), 8.32–8.31 (m, 1H), 8.17–8.16 (m, 1H), 7.82–7.81 (m, 1H), 7.63–7.61 (m, 1H), 7.45–7.43 (m, 1H), 6.88–6.82 (m, 1H), 6.78–6.72 (m, 1H), 6.10–6.08 (m, 1H), 5.87–5.84 (m, 1H), 4.60 (s, 3H, CH_3). **^{13}C-NMR** (acetone-d^6, 100 MHz). δ (ppm) = 167.60, 164.98, 162.87, 162.39, 162.27, 155.79, 155.73, 152.31, 151.29, 151.02, 150.71, 147.47, 147.42, 138.14, 138.10, 128.40, 128.06, 125.84, 125.45, 125.25, 125.02, 124.81, 123.78, 123.14, 122.75, 122.60, 115.51, 114.84, 114.81, 114.67, 114.64, 114.08, 114.05, 113.90, 113.87, 113.48, 99.42, 99.15, 98.88, 98.72, 98.45, 98.18, 42.23 (CH_3). **ESI-MS** (m/z, CH_3CN): $[M^+]$ = 852; $[M^-]$ = 145. Y = 0.098 g (65%). Anal. calcd for $C_{32}H_{16}N_9F_{13}P_1Ir_1$ (996.7) C 38.56, H 1.62, N 12.56. Found: C 37.92, H 1.64, N 12.06.

OLED device fabrication

OLEDs were fabricated by growing a sequence of thin layers on clean glass substrates pre-coated with a 120 nm-thick layer of indium tin oxide (ITO) with a sheet resistance of 20 Ω per square. A 40 nm thick hole injecting layer of poly(3,4-ethylenedioxythiophene) polystyrene sulfonate (PEDOT:PSS, Clevios P VP AI 4083) was spin-coated (4000 rpm) and then the substrates were placed in an oven at 140 °C for 10 min. After the ITO/PEDOT:PSS substrates were cooled down, a 40 nm-thick film of the emitting layer composed of 8 wt% of **[Ir(F$_2$ppy-**

 This journal is © The Royal Society of Chemistry 2025

Open Access Article. Published on 13 May 2025. Downloaded on 7/11/2025 6:28:05 AM. This article is licensed under a Creative Commons Attribution-NonCommercial 3.0 Unported Licence.

CN)$_2$(PTZ)] and 92 wt% of 4,4′,4″-tris(*N*-carbazolyl-triphenylamine) (TCTA) was spin-coated (2000 rpm) in a clean room environment from a 10 mg mL^{-1} dichloromethane solution. An electron transporting layer of 30 nm-thick 2,2′,2″-(1,3,5-benzinetriyl)-tris(1-phenyl-1-*H*-benzimidazole) (TPBi) and a cathode electrode of 0.5 nm-thick LiF with a cap of 100 nm-thick Al were deposited in succession by thermal evaporation under a vacuum of ~10^{-6} hPa. The current–voltage characteristics were measured with a Keithley source-measure unit, model 236, in continuous operation mode, while the light output power was measured with an EG&G power meter and electroluminescence spectra were recorded using a StellarNet spectroradiometer. All measurements were carried out at room temperature under an argon atmosphere and were reproduced for many runs, excluding any irreversible chemical and morphological changes in the devices.

X-ray crystallography

Crystal data and collection details for **[Ir(ppyCN)$_2$(PTZ-CF$_3$)]·*solv*** are reported in Table S1.† The diffraction experiments were carried out on a Bruker APEX II diffractometer equipped with a PHOTON2 detector and using Mo-Kα radiation. Data were corrected for Lorentz polarization and absorption effects (empirical absorption correction SADABS).[22] The structures were solved by direct methods and refined using full-matrix least-squares based on all data using F^2.[23] H-atoms were placed in calculated positions and refined isotropically using a riding model. All non-hydrogen atoms were refined with anisotropic displacement parameters. The unit cell contains an additional total potential solvent-accessible void of 1059 Å^3, corresponding to 1–2 solvent molecules per unit formula. These solvent molecules are highly disordered and, therefore, these voids were treated using the SQUEEZE routine of PLATON.[24a,b] An alert of level A is present in the check-cif. This is due to high values for the residual electron density. This maximum is located close to the Ir atom, in a position which is not realistic for any atom. This is a series termination error, as often found in structures containing heavy atoms. Crystallographic data for the structure reported here has been deposited at the Cambridge Crystallographic Data Centre (CCDC), with CCDC number 2411033.†

DFT calculations

The simulations reported in this work have been performed using the long range corrected hybrid functional (CAM-B3LYP)[25] with Gaussian 1 [26] and ORCA (6.0.1).[27] For the Gaussian calculations, we used the Stuttgart–Dresden (SDD) effective core potential for Ir(III) and the 6-311G** basis set for all other atoms, while for the ORCA calculations, we used the larger def2-TZVP basis set[28] and the D4 van der Waals correction.[29] The effect of the solvent was mimicked using the self-consistent reaction field model (SCRF)[30] in Gaussian and the CPCM[31] method in ORCA, with parameters suitable for acetonitrile. The geometry of all complexes was relaxed with "tight" optimization criteria, and the vibrational frequencies were computed to verify that there were no imaginary frequencies and the minimum energy state was reached. The relaxed structures were then used to perform TD-DFT calculations[32] to compute the absorption spectra. To obtain HOMO–LUMO gap values consistent with the electrochemical measurements, we mimicked the experiments by adding and removing one electron from the complex. The structures were further relaxed in the implicit solvent to model the fact that electrochemistry experiments have much longer time scales than photochemical measurements and therefore such molecular geometry is found as ample time is needed to relax to its new minimum energy configuration. The HOMO–LUMO gap was then computed as:

$$\Delta E_{\mathrm{gap}} = \mathrm{EA} - \mathrm{IP}$$

where EA and IP are the electron affinity and the ionization potential, respectively. The electron affinity was computed as the energy of the reduced state minus the energy of the initial state, and it is assumed to correspond to the energy of the LUMO. The ionization potential was computed as the energy of the oxidized state minus the energy of the initial state and it was assumed to correspond to the negative of the HOMO energy. It has also been shown that typical DFT underestimates the energy gap due to error in the exchange and correlation functionals, but the long range corrected functionals, such as the one used here, are among the best performers.[33]

Author contributions

Conceptualization: V. F., S. S., and M. M; methodology: V. F., N. M., M. C., M. M, P. R., and S. Z.; validation, V. F., M. C., N. M., and S. S.; formal analysis, V. F., N. M., S. S., and M. C.; investigation, data curation, and writing – original draft preparation: N. M., V. F., G. V., E. P., P. R., F. T., M. C., S. Z., and S. S.; review and editing: V. F. and S. S.; visualization: V. F. and S. S.; supervision, V. F., M. M., S. S., L. G., and M. C.; funding acquisition: L. G. All authors have read, edited, and agreed to the published version of the manuscript.

Data availability

All relevant data are within the manuscript and its additional files.

Conflicts of interest

There are no conflicts to declare.

Acknowledgements

The authors wish to thank the Toso Montanari Foundation for financial support.

Open Access Article. Published on 13 May 2025. Downloaded on 7/11/2025 6:28:05 AM.
This article is licensed under a Creative Commons Attribution-NonCommercial 3.0 Unported Licence.

References

1 C. Caporale and M. Massi, *Coord. Chem. Rev.*, 2018, **363**, 71–91.
2 (*a*) D. A. Nicewicz and D. W. C. MacMillan, *Science*, 2008, **322**, 77–80; (*b*) M. A. Ischay, M. E. Anzovino, J. Du and T. P. Yoon, *J. Am. Chem. Soc.*, 2008, **130**, 12886–12887; (*c*) M. R. Narayanam, J. W. Tucker and C. R. J. Stephenson, *J. Am. Chem. Soc.*, 2009, **131**, 8756–8757; (*d*) G. Vigarani, E. Marchini, E. Previati, L. Giorgini, S. Zacchini, R. Argazzi, M. Massi, V. Fiorini, S. Caramori and S. Stagni, *Chem. – Eur. J.*, 2024, **30**, e202400393.
3 A. R. B. M. Yusoff, A. J. Huckaba and M. K. Nazeeruddin, Phosphorescent Neutral Iridium(III) Complexes for Organic Light-Emitting Diodes, in *Photoluminescent Materials and Electroluminescent Devices. Topics in Current Chemistry Collections*, ed. N. Armaroli and H. Bolink, Springer, Cham, 2017.
4 D. Ma, T. Tsuboi, Y. Qiu and L. Duan, *Adv. Mater.*, 2017, **29**, 1603253.
5 L. Flamigni, A. Barbieri, C. Sabatini, B. Ventura and F. Barigelletti, *Top. Curr. Chem.*, 2007, **281**, 143–203.
6 (*a*) J. C. Deaton and F. N. Castellano, Archetypal Iridium(III) Compounds for Optoelectronic and Photonic Applications: Photophysical Properties and Synthetic Methods, in *Iridium(III) in Optoelectronic and Photonics Applications*, ed. E. Zysman-Colman, Wiley-VHC, Weinheim, Germany, 2017, pp. 1–70, and references cited herein; (*b*) J. Frey, B. F. E. Curchod, R. Scopellitti, I. Tavernelli, U. Rothlisberger, M. K. Nazeeruddin and E. Baranoff, *Dalton Trans.*, 2014, **43**, 5667; (*c*) S. Yoon and T. S. Teets, *Chem. Commun.*, 2021, **57**, 1975–1988.
7 (*a*) S. Stagni, E. Orselli, A. Palazzi, L. De Cola, S. Zacchini, C. Femoni, M. Marcaccio, F. Paolucci and S. Zanarini, *Inorg. Chem.*, 2007, **46**, 9126–9138; (*b*) S. Stagni, A. Palazzi, S. Zacchini, B. Ballarin, C. Bruno, M. Marcaccio, F. Paolucci, M. Monari, M. Carano and A. J. Bard, *Inorg. Chem.*, 2006, **45**, 695–709.
8 (*a*) M. V. Werrett, S. Muzzioli, P. J. Wright, A. Palazzi, P. Raiteri, S. Zacchini, M. Massi and S. Stagni, *Inorg. Chem.*, 2014, **53**, 229–243; (*b*) M. V. Werrett, G. S. Huff, S. Muzzioli, V. Fiorini, S. Zacchini, B. Skelton, A. Maggiore, J. M. Malicka, M. Cocchi, K. C. Gordon, S. Stagni and M. Massi, *Dalton Trans.*, 2015, **44**, 8379; (*c*) V. Fiorini, A. M. Ranieri, S. Muzzioli, K. D. M. Magee, S. Zacchini, N. Akabar, A. Stefan, M. I. Ogden, M. Massi and S. Stagni, *Dalton Trans.*, 2015, **44**, 20597.
9 S. Stagni, S. Colella, A. Palazzi, G. Valenti, S. Zacchini, F. Paolucci, M. Marcaccio, R. Q. Albuquerque and L. De Cola, *Inorg. Chem.*, 2008, **47**, 10509–10521.
10 (*a*) V. Fiorini, A. D'Ignazio, K. D. M. Magee, M. I. Ogden, M. Massi and S. Stagni, *Dalton Trans.*, 2016, **45**, 3256–3259; (*b*) V. Fiorini, S. Zacchini, P. Raiteri, R. Mazzoni, V. Zanotti, M. Massi and S. Stagni, *Dalton Trans.*, 2016, **45**, 12884–12896; (*c*) V. Fiorini, I. Zanoni, S. Zacchini, A. L. Costa, A. Hochkoeppler, V. Zanotti, A. M. Ranieri, M. Massi, A. Stefan and S. Stagni, *Dalton Trans.*, 2017, **46**, 12328–12338.
11 N. Miyaura and A. Suzuki, *J. Chem. Soc., Chem. Commun.*, 1979, 866–867.
12 M. Nonoyama, *Bull. Chem. Soc. Jpn.*, 1974, **47**, 767.
13 K. Nakamura, *Bull. Chem. Soc. Jpn.*, 1982, **55**, 2697–2705.
14 C. M. Cardona, W. Li, A. E. Kaifer, D. Stockdale and G. C. Bazan, *Adv. Mater.*, 2011, **23**, 2367–2371.
15 E. Longhi and L. De Cola, Iridium(III) Complexes for OLED Appication, in *Iridium(III) in Optoelectronic and Photonics Applications*, ed. E. Zysman-Colman, Wiley-VHC, Weinheim, Germany, 2017, pp. 205–274, and references cited herein.
16 M. Cocchi, J. Kalinowski, S. Stagni and S. Muzzioli, *Appl. Phys. Lett.*, 2009, **94**, 083306.
17 M. V. Werrett, G. S. Huff, S. Muzzioli, V. Fiorini, S. Zacchini, B. W. Skelton, A. Maggiore, J. M. Malicka, M. Cocchi, K. C. Gordon, S. Stagni and M. Massi, *Dalton Trans.*, 2015, **44**, 8379.
18 G. A. Crosby and J. N. Demas, *J. Phys. Chem.*, 1971, **75**, 991–1024.
19 D. F. Eaton, *Pure Appl. Chem.*, 1988, **60**, 1107–1114.
20 R. N. Butler, Tetrazoles, in *"Comprehensive Heterocyclic Chemistry II"*, ed. R. C. Storr, Pergamon Press, Oxford, U.K., 1996, vol. 4, pp. 621–678, and references cited therein.
21 K. Koguro, T. Oga, S. Mitsui and R. Orita, *Synthesis*, 1998, 910–914.
22 G. M. Sheldrick, *SADABS-2008/1 - Bruker AXS Area Detector Scaling and Absorption Correction*, Bruker AXS, Madison, Wisconsin, USA, 2008.
23 G. M. Sheldrick, *Acta Crystallogr., Sect. C:Struct. Chem.*, 2015, **71**, 3.
24 (*a*) A. L. Spek, *J. Appl. Crystallogr.*, 2003, **36**, 7–13; (*b*) A. L. Spek, *Acta Crystallogr., Sect. D:Biol. Crystallogr.*, 2009, **65**, 148–155.
25 T. Yanai, D. P. Tew and N. C. Handy, *Chem. Phys. Lett.*, 2004, **393**, 51–57.
26 M. J. Frisch, G. W. Trucks, H. B. Schlegel, G. E. Scuseria, M. A. Robb, J. R. Cheeseman, G. Scalmani, V. Barone, G. A. Petersson, H. Nakatsuji, X. Li, M. Caricato, A. V. Marenich, J. Bloino, B. G. Janesko, R. Gomperts, B. Mennucci, H. P. Hratchian, J. V. Ortiz, A. F. Izmaylov, J. L. Sonnenberg, D. Williams-Young, F. Ding, F. Lipparini, F. Egidi, J. Goings, B. Peng, A. Petrone, T. Henderson, D. Ranasinghe, V. G. Zakrzewski, J. Gao, N. Rega, G. Zheng, W. Liang, M. Hada, M. Ehara, K. Toyota, R. Fukuda, J. Hasegawa, M. Ishida, T. Nakajima, Y. Honda, O. Kitao, H. Nakai, T. Vreven, K. Throssell, J. A. Montgomery Jr., J. E. Peralta, F. Ogliaro, M. J. Bearpark, J. J. Heyd, E. N. Brothers, K. N. Kudin, V. N. Staroverov, T. A. Keith, R. Kobayashi, J. Normand, K. Raghavachari, A. P. Rendell, J. C. Burant, S. S. Iyengar, J. Tomasi, M. Cossi, J. M. Millam, M. Klene, C. Adamo, R. Cammi, J. W. Ochterski, R. L. Martin, K. Morokuma, O. Farkas, J. B. Foresman and D. J. Fox, *Gaussian 16, Revision C.01*, Gaussian, Inc., Wallingford CT, 2019.

This journal is © The Royal Society of Chemistry 2025

Open Access Article. Published on 13 May 2025. Downloaded on 7/11/2025 6:28:05 AM.
This article is licensed under a Creative Commons Attribution-NonCommercial 3.0 Unported Licence.

27 F. Neese, Software update: the ORCA program system, version 5.0 WIRES, *Comput. Molec. Sci.*, 2022, **12**(1), e1606, DOI: **10.1002/wcms.1606**.
28 (*a*) F. Weigend and R. Ahlrichs, *Phys. Chem. Chem. Phys.*, 2005, **7**, 3297; (*b*) F. Weigend, *Phys. Chem. Chem. Phys.*, 2006, **8**, 1057.
29 U. Ekstrom, L. Visscher, R. Bast, A. J. Thorvaldsen and K. Ruud, *J. Chem. Theory Comput.*, 2010, **6**, 1971–1980.
30 G. Scalmani and M. J. Frisch, *J. Chem. Phys.*, 2010, **132**, 114110.
31 M. Garcia-Rates and F. Neese, *J. Comput. Chem.*, 2020, **41**, 922–939.
32 F. Neese and G. Olbrich, *Chem. Phys. Lett.*, 2002, **362**, 170.
33 T. Tsuneda, J.-W. Song, S. Suzuki and K. Hirao, *J. Chem. Phys.*, 2010, **133**, 174101.